

Modulated magnetism in PrPtAl

G. Jabbar,¹ D.A. Sokolov,¹ C. O'Neill,¹ C. Stock,¹ D. Wermeille,² F. Dremmel,³
F. Krüger,^{3,4} A.G. Green,⁴ F. Lévy-Bertrand,⁵ B. Grenier,⁶ and A. Huxley¹

¹*School of Physics and CSEC, University of Edinburgh, Edinburgh EH9 3JZ, UK*

²*XMAS, ESRF, BP220, F-38043, Grenoble, France*

³*ISIS, STFC, Rutherford Appleton Laboratory, Chilton, Didcot OX11 0QX, UK*

⁴*London Centre for Nanotechnology, University College London, Gordon St., London WC1H 0AH, UK*

⁵*CNRS, Institut Neel, Grenoble 38042 cedex 9, France*

⁶*Université Joseph Fourier & ILL, Grenoble 38042 cedex 9, France*

(Dated: August 18, 2014)

The transition between paramagnetism and ferromagnetism is the paradigm for a continuous phase transition at finite temperature. When such a transition is tuned to zero temperature, the growth of low energy zero-point fluctuations potentially drives an array of phenomena, including the formation of novel states such as non-conventional superconductivity. Experimentally, the growth of the fluctuations is however curtailed and the transition becomes discontinuous as its temperature is reduced. This is understood to arise from non-analytic corrections to the free energy that always occur. Recent theory suggests that another outcome is also possible with the non-analytic corrections instead forming modulated states. Here, we report the discovery of modulated order in PrPtAl, consistent with complex spirals at the boundary between paramagnetism and ferromagnetism that is the first clear experimental realisation of such a state.

The key idea underlying modulated state formation by the above mechanism is that deformations of the Fermi surface enlarge the phase-space available for low energy particle-hole fluctuations and self-consistently lower the free energy. The fermionic description close to a ferromagnetic quantum critical point [1] has only recently been extended to include coupling to local moments [2], although it has long been realised that local moment physics can be an important source of anisotropy [3]. Although previous theory for spiral formation [4, 5] has considered isotropic magnets, easy plane systems are better candidate materials, since a hard magnetic axis provides a natural orientation for the spiral wavevector and suppresses ‘unwanted’ moment fluctuations along the spiral direction.

Here we describe our findings for PrPtAl. This material is close to being an easy plane ferromagnet, but has an additional magnetic anisotropy between the two easy axes in the plane. The electronic levels of the Pr-seodymium $5f^2$ Pr^{3+} ions are split in the crystal environment (PrPtAl has an orthorhombic TiNiSn structure) into 9 non-magnetic singlet states. Inelastic neutron studies [6] reveal clear crystal field excitations between

these. Choosing a system with only singlets simplifies the theory considerably, avoiding Kondo lattice physics, while still introducing magnetic anisotropy.

Since there are no preformed moments, ferromagnetic order is achieved by mixing singlets via an inter-site exchange interaction [7], a process referred to as *induced moment magnetism*. Our theoretical approach to analysing the magnetic interactions that bring about magnetic order in PrPtAl differs from the standard treatment [8] by keeping the full frequency dependence of the fermion mediated RKKY interaction. This is the key element for a description approaching a quantum critical point and is needed to capture the long wavelength, low energy behaviour of the Free energy expressed as a functional of the local magnetisation. The final result, apart from the inclusion of anisotropy, turns out to be similar to that for a fully itinerant system, but with the ‘local’ moments magnifying the magnetic response.

PrPtAl is reported in the literature to be a simple induced moment ferromagnet [6, 9] with a single transition from paramagnetism to ferromagnetism. Previous scattering studies [6] correctly established that the Pr moments within the unit cell sum to give ferromagnetic order at low temperature (total moment directed along the a -axis), but with the four moments within a unit cell canted in opposing directions in the ac -plane. These measurements however did not look at temperatures around T_{Curie} and macroscopic measurements were made in an applied magnetic field, which obscures a much richer underlying phase diagram that we report below.

In zero magnetic field, we have found that rather than a simple transition from paramagnetism to ferromagnetism there are three consecutive transitions. With decreasing temperature the first is at $T_1 = 5.85 \pm 0.05$ K to a doubly modulated incommensurate state (SDW1), followed by a second transition in the temperature range 5.7-5.3 K (centred at $T_2 = 5.5 \pm 0.1$ K) to a single incommensurate modulation (SDW2) of different period with a strong 3rd order harmonic. The third transition is to uniform ferromagnetism over the temperature interval 5.0-4.3 K (centred at $T_{\text{FM}} = 4.7 \pm 0.1$ K). This is seen in all 4 samples we have studied with neutron scattering (at D23, ILL and SPINS, NIST) and with resonant X-ray scatter-

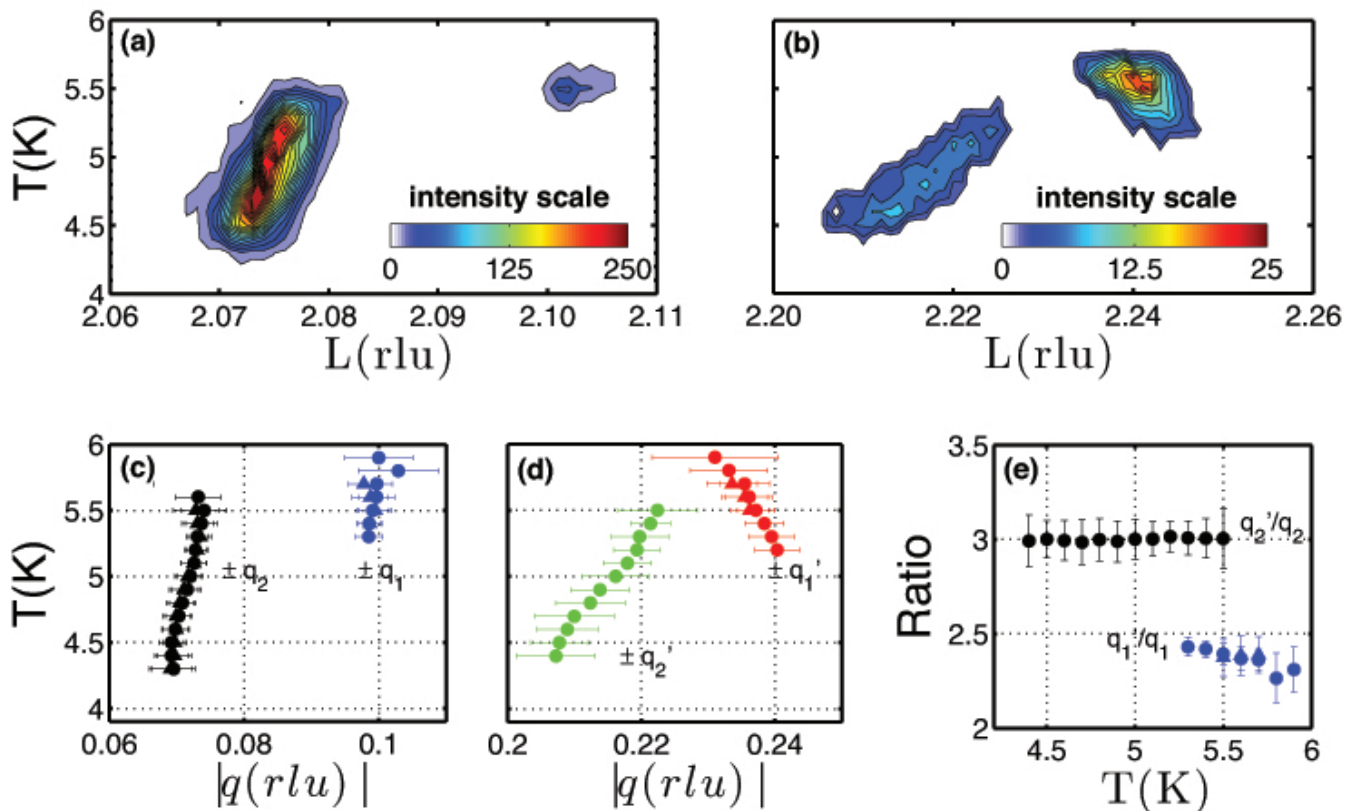


FIG. 1. (a) and (b) are colour-scale images of diffracted intensity as a function of reciprocal coordinate $(0, 0, L)$ and temperature for 6.444 keV X-rays. (c) and (d) are the modulation wavevectors q as a function of temperature deduced from (a) & (b) (circles) and for the symmetric satellites at positions $(0, 0, L) = (0, 0, 2) - (0, 0, q)$ (triangles). q_1 and q_1' are associated with SDW1. q_2 and q_2' are associated with SDW2. Panel (e) shows the ratio of modulation vectors.

ing (BM28, ESRF). Data obtained with resonant X-ray scattering have the highest q -resolution and are shown in FIG 1. The incommensurate diffraction signal is visible for a X-ray energy at the Pr L_2 resonance edge (6.444 keV), which fluorescence and absorbance measurements suggest is a simple dipole transition. The observed intensity in neutron scattering at the same wavevector-transfer prove that the satellites are of magnetic origin. In both SDW states the modulation vectors are precisely along the c -axis.

To further explore the nature of magnetic order we measured the spin-dependence of the neutron cross-section at wave-vector transfer $(0, 0, 2 \pm q)$ with the SPINS instrument at NIST. Incoming neutron spin polarisation was aligned with the crystal \mathbf{a} -axis. In the SDW2 state ($q \approx 0.07$ r.l.u.) spin-flip (SF) scattering was observed with an intensity 0.1 times that for non spin-flip (NSF) scattering. This implies that the modulated state has magnetic moments along the \mathbf{b} -axis as well as along the \mathbf{a} -axis. This suggests the SDW2 states could be an elliptical spiral.

The examination of the SF/NSF ratio for satellites close to other Bragg positions revealed that there is also a moment component along the \mathbf{c} -axis (parallel to \mathbf{q}) (Sup-

plementary Information). A magnetic structure for the SDW2 state consistent with these measurements is shown in FIG 2. In the figure the moments rotate in a plane whose normal is inclined from the propagation direction. In addition there is an intra-cell antiferromagnetic moment (equivalent to that in the FM state), which for clarity is not shown.

The presence of third order harmonics for SDW2 provides further indirect evidence for spiral order. The moment direction for a simple spiral propagating along the \mathbf{z} direction with moments turning in the \mathbf{xy} plane in presence of crystalline anisotropy can be written

$$\frac{1}{|m|} \begin{pmatrix} m_x \\ m_y \end{pmatrix} = \begin{pmatrix} \cos[q_m z - \phi(z)] \\ \sin[q_m z - \phi(z)] \end{pmatrix} \quad (1)$$

with q_m the principal modulation vector. The phase $\phi(z)$ allows the pitch of the spiral to vary with position to reduce the anisotropy energy. In this expression $\phi(z)$ is periodic with period π/q_m resulting in only odd harmonic components of the amplitude of the magnetisation with $q = (2n + 1)q_m$ (for integer n). For example, in a weak ellipsoidal (2-fold) anisotropy the free-energy is minimised for $\phi(z) = \delta \sin(2q_m z)$ resulting in a third order amplitude $\delta/2$. A strong 4-fold anisotropy is re-

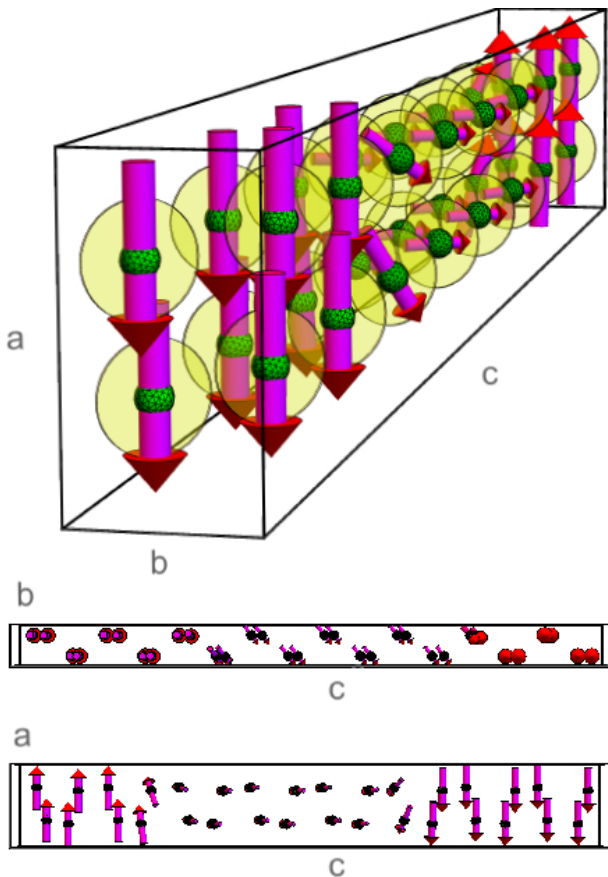


FIG. 2. (a) Image of the SDW2 state over a length of approximately $1/2$ the modulation period. Only the Pr atoms are shown. These form chains running along the c -axis with different a -coordinate, zig-zagging in the bc -plane. There is an additional intra-cell canting that tilts the moments out the plane of the shaded discs in the $\pm c$ -direction (in the opposite sense in adjacent chains) which for clarity is not shown. The lower panels show the same structure as in the upper panel viewed from the a and b -directions.

quired to explain the experimentally measured SF and NSF third harmonic intensities for PrPtAl.

The changes of magnetic structure seen with diffraction also have signatures in thermodynamic measurements that we now describe, starting with the heat capacity. The heat capacity divided by temperature C/T has cusp-like features at all three transitions (FIG 3). The scatter in values at T_{FM} and T_2 depend on the temperature history indicating that these transitions are almost certainly first order. C/T extrapolates to a large value of around $40 \text{ mJ mole}^{-1}\text{K}^{-2}$ at low temperature. This is consistent with a large electronic effective mass that could arise from a strong interaction between conduction electrons and local moments. A strong local-moment conduction-electron interaction supports the order by disorder mechanism for modulated state formation described later.

The dc susceptibility, namely magnetisation divided by the applied magnetic field (M/H), and ac susceptibility (χ) are also shown in FIG 3. The SDW2 state is clearly much less strongly polarisable than both SDW1 and FM. The distinct signatures of the modulated state in magnetisation measurements are suppressed with field being washed out in a field of only 10 mT (this explains why the modulated states were missed in some earlier studies). An out of phase component of the ac-susceptibility χ'' develops only below the lowest transition with a corresponding reduction of the in phase susceptibility χ' relative to M/H . This marks the onset of dissipation (hysteresis) due to the formation of ferromagnetic domains.

We now examine possible explanations for the formation of the modulated states, considering firstly two mechanisms that can be described in terms of local moment physics alone.

The first applies when there is no inversion symmetry; the resulting Dzyaloshinski-Moriya interaction then favours spiral magnetic order [10] as found in MnSi [11]. For PrPtAl there are crystal inversion symmetries linking Pr sites and therefore there is no such interaction between them.

The second mechanism arises from competing near neighbour exchange interactions, that can be tuned to give a Devil's staircase of large period commensurate ordering vectors [12], describing periodic patterns of domain walls. The theory has been suggested to apply to holmium metal [13] where the moments rotate from one hexagonal plane of the structure to the next with a quasi-continuous evolution of q with decreasing temperature, before q locks to a fixed value at lower temperature. The absence of dissipation in the a.c. susceptibility in the SDW2 and SDW1 phases and our observation that neutron spin depolarisation was only found below T_{FM} (Supplementary Information) rule out domain wall based explanations for the modulated structures in PrPtAl. The q -vector in PrPtAl also evolves continuously.

We now discuss explanations for the modulated states that depend more explicitly on the conduction electrons. Our observations for PrPtAl invite comparison with hexagonal Tb and Dy. Both Tb and Dy have modulated magnetic states below an ordering temperature T_N and undergo first order transitions at lower temperatures to uniform ferromagnetism [14]. We briefly describe the various theories that have been put forward for Tb and Dy and how the magnetism of PrPtAl is different.

The theories for Tb and Dy consider a long-range exchange interaction $J(q)$ between magnetic ions transmitted by the conduction electrons (known as the RKKY interaction) that is peaked at an initial ordering vector. As the temperature is lowered below T_N the effect of magnetic anisotropy grows as a strong power of the ordered moment [15], leading to a reduction of the ordering wave-vector and then a transition to ferromagnetism. The peak in $J(q)$ has been attributed to either a nesting

of the Fermi-surface [16] or a Kohn anomaly [17]. In both cases the magnetic super-zone cell in the modulated state reduces the electronic density of states and contributes to lowering the energy in mean field theory. The theories have been reasonably successful in explaining the qualitative temperature evolution $q(T)$. Similar behaviour to Tb and Dy is also reported in some samples of UCu_2Si_2 [18]; in this case Kondo physics may be involved as well as Fermi-surface nesting [19].

Substantial Fermi-surface nesting for a 3D material is extremely rare. One example is found in α -uranium [20] where it gives rise to a charge density wave, rather than to a spin density wave. For the rare earth elements, including Tb and Dy, a webbing feature at the zone boundary specific to their hexagonal crystal structure may provide such a special case [16]. The band structure for PrPtAl is not known, but that for LaPtAl [21] provides a guide considering the Pr f-electrons to be localised. For LaPtAl there are no apparent nesting vectors along the c -direction. Nesting is therefore unlikely to underlie modulated state formation in PrPtAl.

For the SDW1 state q_1' increases with decreasing temperature which is the opposite trend from the above materials. We focus our discussion on the SDW2 state that spans a wider temperature interval. The temperature dependence and magnitude of $q_2(T)$ is similar to $q(T)$ for the rare earths, but there are important differences in other quantities. For both Dy [22] and Tb [23] there is a marked increase of electrical resistance entering the modulated state when the electrical current is parallel to the modulation vector. This is explained by the formation of a super-zone cell, which gaps the Fermi-surface and therefore reduces the density of states. FIG 4 shows that for PrPtAl in contrast the resistivity falls with decreasing temperature. There is a small hysteresis of up to 1% between the values of resistance in the ordered state below T_{c1} . The value in increasing temperature is lower than in decreasing temperature, confirming that states PM, SDW1, SDW2 and FM have successively *lower* resistivity. Another difference from the rare earth elements concerns the behaviour in a magnetic field applied along the easy-axis (the \mathbf{a} -axis), which we describe next.

For hexagonal Tb and Dy there is a transition from a helix to a fan state and then to ferromagnetism with magnetic field. The field at which the upper transition occurs depends on the temperature but has a maximum value near T_N of around 1 T for Dy [24] and 0.5 T for Tb [25]. For the above theory the transition field is expected to be of the order $(J(0) - J(q))/\mu$ [26] in agreement with the observed fields (μ is the magnetic moment). For PrPtAl the energy dispersion of the lowest crystal field excitation gives an energy difference $E(0) - E(q_{1,2}) \approx 0.2$ meV (Supplementary Information), which corresponds to a field in excess of 2 T.

FIG 4 shows the magneto-resistance at different temperatures. A strong negative MR is characteristic of the

suppression of critical fluctuations with magnetic field. The expected initial dependence is quadratic with field in the paramagnetic state, but can be linear with field in an ordered state. It is then striking that over the range of temperatures where SDW1 occurs the initial magneto-resistance (MR) is positive passing through a peak at around 10 mT before becoming negative at higher magnetic field. A positive MR may indicate the formation of higher order super-zone gaps [28]. This then suggests that the SDW1 structure is suppressed by a modest field of only 10 mT. At temperatures where only SDW2 is present the MR is negative at a much lower field which suggests that the critical field to suppress this state is lower. The suppression of the features in the magnetisation below 10 mT was already commented on (FIG 3). These changes at very low magnetic field suggest that the modulated state in PrPtAl is very rapidly suppressed, well below 2 T and therefore requires a different description from that used for the modulated states in the rare earth elements.

Below we show that non-analyticities of the free energy approaching quantum criticality can explain our findings of extreme sensitivity to magnetic field and a fall in resistivity on entering the modulate states. Such a transition to modulated states is predicted on general grounds when the Curie temperature is small. Moreover the ordering vector does not have to match any special feature of the Fermi-surface geometry.

The long-wavelength model consists of conduction electrons at chemical potential μ , interacting via a local repulsion g and coupled to the local moments \mathbf{J} of the Pr^{3+} ions with coupling constant γ . The Hamiltonian is

$$H = \int_{\mathbf{r}} \left\{ (\psi_{\uparrow}^{\dagger}, \psi_{\downarrow}^{\dagger}) \left[-\nabla^2 - \mu - \gamma \sum_{\alpha} J_{\alpha}(\mathbf{r}) \sigma_{\alpha} \right] \begin{pmatrix} \psi_{\uparrow} \\ \psi_{\downarrow} \end{pmatrix} + g \psi_{\uparrow}^{\dagger} \psi_{\uparrow} \psi_{\downarrow}^{\dagger} \psi_{\downarrow} + \frac{1}{2} \sum_{\alpha} \chi_{\alpha}^{-1} J_{\alpha}^2(\mathbf{r}) \right\}, \quad (2)$$

where σ_{α} ($\alpha = x, y, z$) denote Pauli matrices and $\psi_{\nu}(\mathbf{r})$ ($\nu = \downarrow, \uparrow$) are electronic field operators. The electron dispersion is taken to be isotropic. Magnetic anisotropy is induced through the van-Vleck susceptibility of the local moments ($\chi_a > \chi_b \gg \chi_c$). In the temperature range where the spiral forms the local susceptibility has a negligible temperature dependence. For sufficiently strong interactions g , the model exhibits a FM ground state with a moment along the \mathbf{a} -axis.

The central idea of the quantum order by disorder approach is to self-consistently compute fluctuations and their contribution to the free energy near the quantum critical point for different magnetically ordered states. This reproduces a non-analytic free energy contribution $\Delta f_0 \sim m^4 \ln(m^2 + T^2)$ for a homogeneous FM state that leads to a first order transition at low temperatures. The first-order transition is however pre-empted by the formation of an incommensurate spiral state. The free-energy

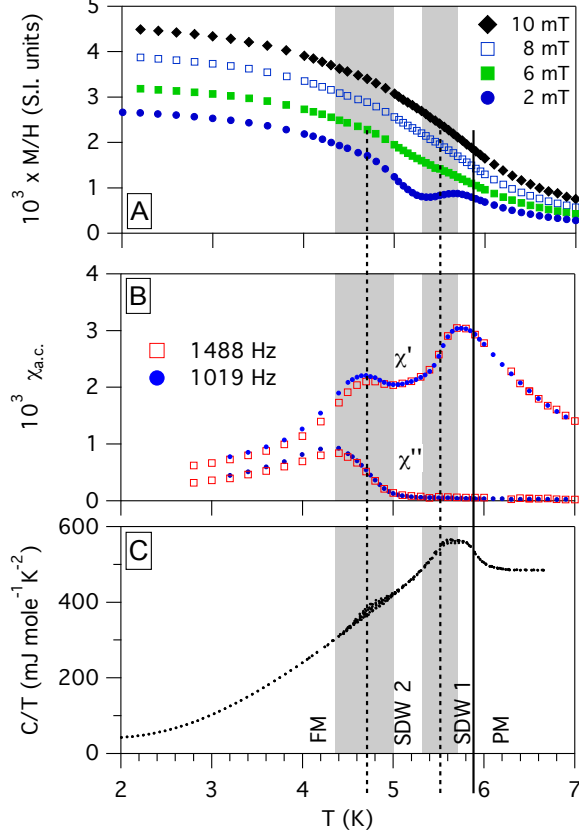


FIG. 3. Thermodynamic measurements for PrPtAl: (A) magnetisation/applied magnetic field (d.c. susceptibility) for field applied along the easy a-axis (B) the in-phase χ' and the out-of-phase χ'' parts of the susceptibility measured in zero magnetic field at frequencies of 1 and 1.5 kHz. (C) the heat capacity divided by temperature. The vertical lines passing through all the panels show the temperature for the transitions seen with neutron and X-ray scattering.

for modulated states can be obtained from the expression for the uniform state by noting that the electron dispersion becomes $\epsilon_{\pm}(\mathbf{k}) = k^2 \pm \sqrt{(k_z q)^2 + (gm)^2}$ in the presence of spiral order. The free energy density is then $f(m, q) = f_0(m) + f_2(m)q^2 + \frac{1}{2}f_4(m)q^4$, where the functions f_2 and f_4 can be deduced from the homogeneous result f_0 (Supplementary Information).

Including the local moments in the above analysis leads to the same free-energy expression plus an additional anisotropy term $f_{\text{anis}}(\mathbf{r}) = \sum_{\alpha} u_{\alpha} m_{\alpha}^2(\mathbf{r})$ with $u_{\alpha} = -2\gamma^2/(\chi_{\alpha}^{-1} + 2\gamma^2/g)$. In this expression \mathbf{m} is the total moment, which is composed of a conduction electron and local moment contribution, $\mathbf{m} = \mathbf{m}_{\text{cond}} + \frac{\gamma}{g}\mathbf{J}$. The local moment is given by $J_{\alpha} = \frac{2\gamma}{\chi_{\alpha}^{-1} + 2\gamma^2/g} m_{\alpha}$.

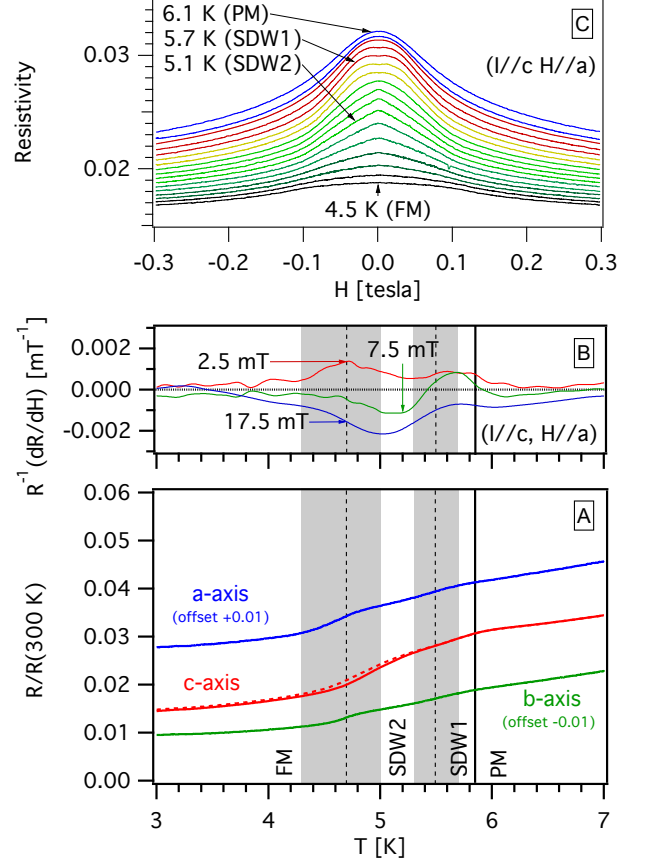


FIG. 4. Resistivity measurements for PrPtAl: (A) the zero field resistivity relative to 300 K for currents in different directions (measurements shown are for increasing temperature, the measurement for decreasing temperature for the c-axis is also shown dashed), (B) the differential magnetoresistance for current in the c-direction and field in the a-direction as a function of temperature, (C) resistance as a function of magnetic field for temperatures in the range 4.5 to 6.1 K in 0.1 K steps ($H//\mathbf{a}$, $I//\mathbf{c}$).

As for the fully itinerant theory, the finite range of the interaction and the effect of weak disorder can be included by introducing two further parameters whose values determine the tri-critical temperature and extent of the modulated region (see Supplementary Information). The resulting phase diagram is shown in FIG 5(a). Over a range of electron interactions g , we find a sequence of transitions upon cooling from a paramagnet to a modulated spiral ($q \parallel \mathbf{c}$) and then to FM ($m \parallel \mathbf{a}$).

A key prediction of the quantum order by disorder model is the increase of the spiral ordering wave vector with temperature (see FIG 5(b)). This behaviour is indeed observed in the modulated phase SDW2. The anisotropy in the \mathbf{ab} -plane renders the FM/spiral tran-

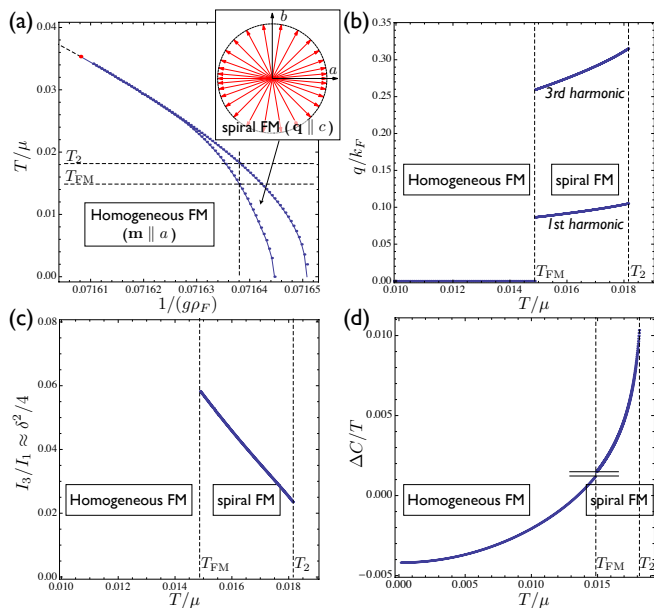


FIG. 5. Theoretical predictions of the quantum order-by-disorder model. (a) Phase diagram as a function of temperature T and inverse electron interaction strength g (ρ_F is the density of states at the Fermi energy). The vertical dashed line shows a value of g that would give transitions with increasing temperature from ferromagnetism to a (spiral) modulated state and then to paramagnetism. The inset shows the dominant anisotropy-induced deformation of the spiral. (b) Evolution of the spiral ordering wavevector q (in units of the Fermi wavevector k_F) as a function of temperature. (c) Intensity ratio I_3/I_1 of third and first harmonics in the spiral phase. (d) Magnetic contribution to the heat capacity, $\Delta C/T$

sition weakly first order with a small change in magnetisation but a relatively big jump of q .

The anisotropy also causes the deformation $\phi(z) = \delta \sin(2qz)$ of the spiral (see FIG 5(b)) as described earlier, giving rise to odd higher harmonics in the magnetic structure factor. As shown in FIG 5(c), we find typical values of 5% for the intensity ratio $I_3/I_1 = \delta^2/4$ between third and first harmonics. The spectral weight of the third harmonic is further enhanced by modulations of the moment magnitude, $m[1 + \delta \cos(2qz)]$, corresponding to an elliptical deformation of the spiral. With increasing anisotropy between **a** and **b** directions, the deformations of the spiral increase slightly up to the point where the spiral phase is destroyed. A more complete description could include crystal field parameters (not currently known) and quantum spin states for the local moment to better accounts for the actual anisotropy as a function of local moment direction.

The calculated magnetic contribution to the specific heat is shown in FIG 5(d). The Sommerfeld coefficient $\Delta C/T$ increases monotonically and shows a sharp drop at the transition to the paramagnet state. The FM-spiral transition is characterised by a small jump, as well as a

latent heat that could explain the scatter in the values of the experimental heat capacity close to T_{FM} .

In the order by disorder model, the instability towards the formation of a modulated spiral state is driven by an enhancement of electronic particle-hole fluctuation due to elliptical Fermi surface deformations and the latter is expected to dominate any reduction in the density of states owing to the formation of superzone gaps. This leads to an increase of the density of states by a factor $[1 + \frac{1}{8} (\frac{q}{k_F})^2]$ which provides an explanation for the resistivity drops in PrPtAl on passing from the paramagnetic to the modulated state. This is in stark contrast with the behaviour expected when spiral states arise from nesting instabilities or Kohn anomalies. In those cases and as observed in Dy, Tb and UCu₂Si₂, the superzone gapping leads to an increase in resistivity.

The energy stabilising the spiral formation relative to ferromagnetism is small and this means that the spirals are very sensitive to an applied magnetic field along the easy-axis. For the above model parameters, a magnetic field of only a few millitesla is sufficient to suppress the modulated state (Supplementary Information).

The modulated state is also predicted to be sensitive to sample quality and would be absent in lower quality samples with shorter mean-free path (Supplementary Information). The heat capacity reported in the literature [27] for arc-melted polycrystals does not show any signature of the modulated states supporting this conclusion.

If quantum criticality indeed underlies the modulated state formation, the range of temperature over which the spiral state exists relative to the ferromagnetic state should increase as T_C is reduced. We have made measurements at different pressures that indeed show this to be the case (Supplementary Information). The transition temperatures rise with pressure and become closer together, which corresponds to an increase of conduction electron interaction, g .

Given the simplicity of the above calculation, its success in accounting for the observed phenomena in PrPtAl is remarkable. A more quantitative comparison requires more detailed knowledge of the band structure and crystalline electric field than currently available. Consideration of multiple bands might then also afford an explanation for the doubly modulated state SDW1.

The induced moment magnet PrPtAl thus provides the first example of modulated state formation at the border between ferromagnetism and paramagnetism, driven by quantum criticality. The phenomena we have observed agree with many of the predictions for quantum critical theory. This validates an interesting alternative to transitions becoming discontinuous approaching the ferromagnetic-paramagnetic QCP. It avoids cutting off the divergence of critical fluctuations, although the divergence is shifted to a finite wavevectors. Such fluctuations are not linked to a Fermi-surface nesting vector

and represent a new type of quantum critical behaviour. The changed nature of the fluctuations may possibly lead to different quantum ordered states emerging at lower temperatures and be relevant to the formation of unconventional superconductivity. In particular even when a modulated state does not form, soft fluctuations associated with incipient modulated state formation, centred at small but finite \mathbf{q} 's, may provide the glue for magnetic pairing.

Supplementary Information

Samples. Single crystals were grown from high purity starting materials (Pr supplied by Ames laboratories, Pt (4N8), and Al (5N) from Alfa Aesar) by Czochralskii pulling from a RF-heated melt in water cooled crucible under UHV/high purity argon.

Elastic neutron scattering. The elastic spin analysed neutron scattering cross-section was measured with the SPINS triple-axis instrument at NIST. 5 meV neutrons were used with cold Be-filters in both incident and scattered paths. The neutrons were polarised with a Fe/Si supermirror and 10' collimator. A 20' collimator - Fe/Si supermirror - 40' collimator prior to a PG002 energy analyser was used for spin analysis of the diffracted neutrons. Spin flippers either side of the sample were used to access both directions of incident and diffracted spins. A guide field of 0.3 mT was applied parallel to the sample \mathbf{a} -axis (vertical). This field is small enough not to affect the modulated states but insufficient to align ferromagnetic domains. At 7 K in the paramagnetic state the ratio of spin-flip (SF) scattering to non spin flip scattering (NSF) was measured to be 19.5 (an average for both (011) and (002) Bragg peaks). Since only nuclear scattering is present, which does not flip the neutron spin, this gives a measure of the polarisation efficiency $P=0.95$. The magnetic scattering amplitudes add to the nuclear scattering amplitude at lower temperature. The beam polarisation was preserved down to 5 K. Below this temperature the beam was progressively depolarised owing to the onset of ferromagnetism and presence of ferromagnetic domains. Here we report measurements in the modulated states above 5 K where there was no depolarisation.

For our geometry with the \mathbf{a} -axis vertical, an \mathbf{a} -axis moment results in non-spin-flip (NSF) scattering, with spin flip (SF) scattering sensitive to the moment component perpendicular to both \mathbf{a} and the total scattering vector \mathbf{Q} . Our study focussed on satellites $(0, 0, 2 \pm \delta)$, $(0, 1, 1 \pm \delta)$ and $(0, 1, 2 \pm \delta)$. An example of the data is shown in FIG 6. An enhanced ratio of SF/NSF scattering for the magnetic satellite compared with the nuclear Bragg peak is clear. For $(0, 0, 2 \pm \delta)$, NSF is only sensitive to moments along the \mathbf{a} -axis and SF to moments along the \mathbf{b} -axis. The ratio of SF/NSF scattering corrected for the polarisation efficiency at different temperatures is

shown in FIG 6. The observation of significant SF scattering unambiguously proves that there must be a component of the moment parallel to the \mathbf{b} -axis in the SDW2 state. This contrasts with the FM state below 5K which has no \mathbf{b} -axis moment. The ratio SF/NSF decreases as the temperature is lowered (FIG 6) indicating that the fractional moment parallel to the \mathbf{b} -axis decreases on approaching the FM state.

The 4 Pr sites in the unit cell are split into two types of site; A and B [29]. The A and B atoms separately form chains along the c -axis. In principle there could be a phase and/or amplitude difference between the moments on the A and B sites. To examine these possibilities we measured scattering at $(0, 1, 2.07)$. We found that for this peak there was no detectable NSF scattering, but a clear SF signal. From this it can be concluded that there is no phase or moment difference between the A and B sites (other than that from the magnetic modulation q) for the moment along the \mathbf{a} -axis. We also examined the scattering at $(0, 1, 1.07)$ to check for an eventual c -axis moment. The SF/NSF ratio was found to be 50% higher at this position than at $(0, 0, 2.07)$. This indicates the presence of a significant c -axis moment at wavevector q .

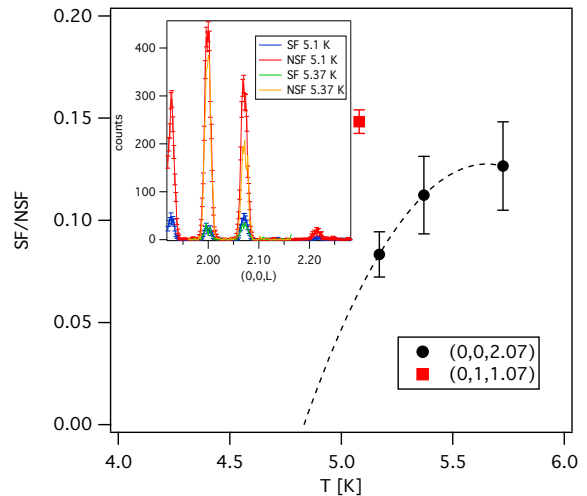


FIG. 6. The main panel shows the temperature dependence of the ratio of spin-flip to non-spin-flip scattering corrected for the polarisation efficiency at $(0,0,2.07)$ and at one temperature for $(0,1,1.07)$. The insert shows typical raw intensity data as a function of q .

X-ray scattering. Resonant X-ray diffraction was carried out at the XMAS UK-CRG beamline (BM28) at the ESRF on natural as grown sample surfaces (crystal mosaic FWHM 0.01°). The energy dependence of the fluorescence and absorption were consistent with a simple dipole transition with a sharp maximum in absorption, fluorescence and magnetic scattering (measured for $(0,0,2.07)$ at 5K) at 6.444 keV close to the standard Pr L_2 edge. This energy was used for the subsequent measure-

ments. Measurement of the scattering intensity shown in FIG 1 were made in a vertical diffraction plane geometry with a LiF (220) analyser set to detect scattering in the $\sigma\pi$ polarisation channel to discriminate against background charge scattering. The temperature dependence of wavevectors q was similar to that observed with SPINS. The X-ray measurements additionally showed that the modulation vectors were all precisely along the \mathbf{c} -axis.

A model structure (averaged over domains) that is consistent with our measurements has moments for all sites with components at the fundamental modulation vector $(\cos(q.r), 0.3 \sin(q.r), \pm 0.4 \sin(q.r))$ plus a staggered moment of opposite sign for the A and B sites $(0, 0, 0.28 \cos(q.r))$. A strong 4-fold modulation is required to give the observed 3rd order harmonics with similar neutron scattering SF/NSF ratios to the fundamental.

Inelastic neutron scattering. An inelastic neutron scattering spectrum was recorded with the OSIRIS time of flight instrument (at ISIS, UK), operated in a standard configuration with PG002 analysers. The crystal was measured with the \mathbf{b} -axis vertical. The scattering spectrum at 2 K is shown in FIG 7. The two dispersing excitations are two branches of the excitation from the ground state singlet to the lowest excited singlet. The difference in energy is $E(0) - E(q) \approx 0.2 \text{ meV}$. This increase to around 0.4 meV at 6 K. Higher q -resolution is needed to identify the exact values of \mathbf{q} at which the minima occurs, but it is in the range of the observed modulation vectors. The overall intensity distribution comes from the structure factor and is reproduced in a standard mean field calculation, although the dip at the modulation vector cannot be captured without including long range interactions.

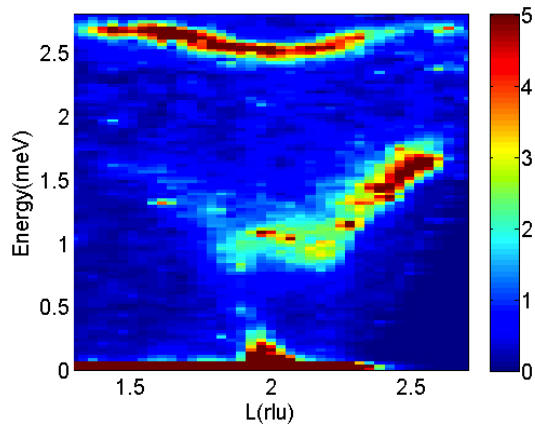


FIG. 7. The dispersion of the lowest energy magnetic excitation measured along $(0,0,L)$ at 2.0 K. The intensity is in arbitrary units.

Pressure study The magnetisation was measured with a small piston cylinder cell inserted into a standard quantum design MPMS magnetometer. The temperature dependence of the magnetisation under pressure was found to have the same form as at zero pressure (FIG 3A). The evolution of the transition temperatures are estimated from the changes in temperature of the inflections of M plotted as a function of T and are shown in FIG 8. T_C increases with pressure and the temperature range over which the modulated state exists decreases, while the temperature range of the modulated states becomes smaller.

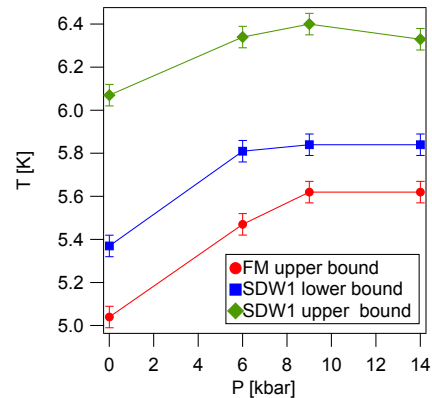


FIG. 8. Phase diagram as a function of pressure. The Figure shows the temperatures of the inflections in the magnetisation at different pressures (see FIG 1). These positions are different from the transition temperatures T_{FM} , T_2 , and T_1 . Their pressure evolution of these features however gives an indication of the evolution of the transition temperatures, from which it is clear that the transitions move to higher temperature and become more bunched with increasing pressure.

Theory. The key steps of the derivation of the free energy are as follows. (i) Starting from a coherent state path integral, we perform a Hubbard-Stratonovich decoupling of the electron interaction term in spin- and charge channels. (ii) We decompose the introduced fluctuation fields into zero- and finite-frequency components. The former correspond to static order in the system. The central step is to include the total magnetisation \mathbf{m} in the free-fermion propagator. This facilitates the self consistent expansion and re-sums classes of diagrams to infinite order. (iii) We trace over the fermions, keeping all terms up to quadratic order in the finite-frequency fluctuation fields. (iv) We perform the Gaussian integrals over the fluctuation fields.

In the case of the homogeneous FM this procedure gives rise to the free energy density [5, 30]

$$f_0(m) = [(g\rho_F)^{-1} + a_2] m^2 + a_4 m^4 + a_6 m^6 + \frac{1}{2} \lambda (g\rho_F)^2 m^4 \ln \left[\kappa m^2 + \left(\frac{T}{\mu} \right)^2 \right], \quad (3)$$

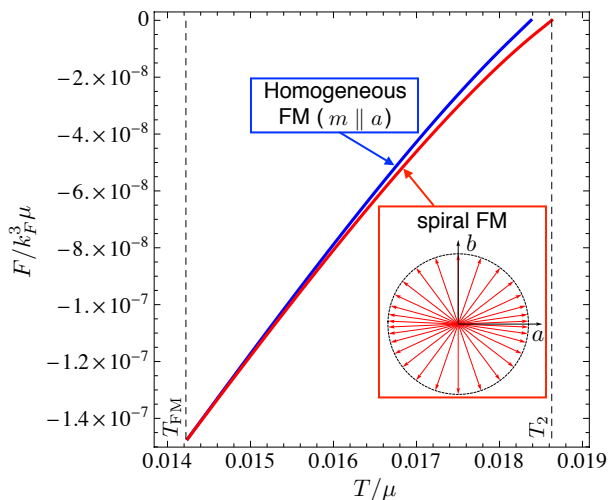


FIG. 9. Free energies of the spiral and homogeneous FM states in the temperature range between T_{FM} and T_2 over which the spiral is stable. The interaction strength is the same as in FIG. 5.

in agreement with the expression first derived by Belitz, Kirkpatrick, and Vojta [1] by a diagrammatic expansion around the paramagnetic state. Here we have rescaled to dimensionless units, $f = F/(\mu k_F^3 V)$, and rescaled the magnetisation, $m \rightarrow (\mu/g)m$. $\rho_F = k_F^3/\mu$ is proportional to the density of states at the Fermi level.

The mean-field (MF) coefficients are given by simple integrals over derivatives of Fermi functions, $a_{2j} = \frac{1}{j(2j-1)!} \int_{\mathbf{k}} n_F^{(2j-1)}(k^2)$. The parameter λ determines the temperature of the tri-critical point, $T_c \sim \exp(-a_4/\lambda)$, the parameter κ controls where the FM first-order line and the spiral/paramagnet phase boundary terminate on the $T = 0$ axis. These parameters can be calculated analytically for the simple model with isotropic electron dispersion and contact repulsion, $\lambda = 16\sqrt{2}/[3(2\pi)^6] \approx 1.2 \cdot 10^{-4}$ [5] and $\kappa = 4$ [30]. Note that this value of κ is obtained from a re-summation of the leading temperature divergences to all orders of m . Taking into account the sub-leading divergences as well, the magnetically ordered region increases considerably [30]. This can be captured by a reduced value of κ .

However, both λ and κ strongly depend on the range of electron interactions, e.g. λ decreases with the interaction range, leading to an exponential suppression of T_c [1, 31]. Since it is not possible to calculate λ and κ for a more realistic model, we instead follow the logic of previous work [31] and determine the parameters from the transition temperatures of PrPtAl. Good agreement is found for $\lambda = 2.3 \cdot 10^{-6}$ and $\kappa = 0.02$. It should be noted that the values of the various parameters are underconstrained with the values for λ and κ depending on the choice for g and μ , but also the quasi-particle mass m^* .

Since m and q enter the free-energy functional always in the same combination through the electron dispersion $\epsilon_{\pm}(\mathbf{k}) = k^2 \pm \sqrt{\hat{k}_z^2 q^2 + m^2}$ (momenta in units of k_F) and since the MF and fluctuation integrals are sharply peaked around the Fermi energy, the finite- q coefficients differ from the homogeneous ones only by combinatorial factors and angular averages over powers of $\hat{k}_z = \cos\theta$. E.g., the $m^2 q^2$ coefficient is proportional to the m^4 coefficient, explaining why the spiral forms below the tri-critical point. The full free energy expression is given by [30]

$$f(m, q) = \frac{1}{2} \int_0^\pi d\theta \sin\theta f_0 \left(\sqrt{\hat{k}_z^2 q^2 + m^2} \right). \quad (4)$$

After expanding in powers of q we obtain lengthy but closed form expressions for the functions $f_2(m)$ and $f_4(m)$.

In the following we estimate the critical field along the magnetic easy \mathbf{a} -axis that is required to suppress the spiral. This field is expected to be small since the quantum fluctuations that lead to the spiral instability are of the same origin as the non-analytic free energy contributions that stabilise FM order beyond the region predicted by mean-field theory. In fact, the transition from the paramagnet into the spiral phase only slightly pre-empts the fluctuation induced first-order transition into the FM. As a result, the free energy difference between the homogeneous and modulated states is very small. It is reduced even further due to the magnetic anisotropy in the easy plane.

For a quantitative estimate we calculate the free energies in the temperature interval over which the spiral is stable. Close to the transition to the paramagnet at T_2 we find a maximum free-energy difference of $\Delta F/V \sim 10^{-8} k_F^3 \mu$ (see FIG. 9). Assuming $k_F^3 \sim 10$ and using $k_B T_c \sim 10^{-2} \mu$ with $T_c \sim 10\text{K}$ we obtain $\Delta F/V \sim 10^{-8} \text{eV}$. Comparing this energy to the energy gained by aligning the uniform state to an applied field yields a critical field strength of $\sim 1\text{mT}$ for a moment of $0.1\mu_B$ close to T_2 . Taking the deformation of the spiral state in a field into account would give a slightly larger estimate for the critical field.

Disorder has crucial effects on the form of the fluctuation corrections to the free energy and therefore on the location of the tri-critical point and the formation of modulated states at temperatures below T_c . It cuts off the logarithmic divergence at low temperatures and leads to a stronger divergence of opposite sign [1, 31]. As a consequence, T_c is reduced by disorder. For strong enough disorder, the fluctuation-induced first-order behaviour and the related instability towards the formation of modulated spiral phases are destroyed. This might be the reason why earlier heat capacity measurements on PrPtAl have not detected the rich structure that we find for clean samples.

acknowledgements Support from the Royal Society (AH),

EPSRC (AH, DS) and SUPA (CS) is gratefully acknowledged.

-
- [1] D. Belitz, T.R. Kirkpatrick & T. Vojta, Phys. Rev. Lett. **82**, 4707 (1999).
- [2] T.R. Kirkpatrick & D. Belitz, Phys. Rev. B **85**, 134451 (2012).
- [3] R. Roussev & A.J. Millis, Phys. Rev. B **61**, 140504R (2001).
- [4] G.J. Conduit, A.G. Green & B.D. Simons, Phys. Rev. Lett. **103**, 207201 (2009).
- [5] U. Karahasanovic, F. Kruger & A.G. Green, Phys. Rev. B **85**, 165111 (2012).
- [6] H. Kitazawa, A. Dönni, L. Keller, J. Tang, F. Fauth & G. Kido, J. Sol. State. Chem. **140**, 233 (1998).
- [7] B. Bleaney, Proc. of the Royal Soc. of London, **A 276**, 19 (1963).
- [8] Jens Jensen and Allan R. Macintosh, Rare Earth Magnetism, Structures and Excitations, Clarendon (Oxford) 1991.
- [9] F. Hullinger, J. of Alloys and Compounds **196**, 225 (1993).
- [10] P. Bak & M.H. Jensen, Phys. C **13**, L881 (1980).
- [11] C. Pappas, E. Lelievre-Berna, P. Falus. et al., Phys. Rev. Lett. **102**, 197202 (2009).
- [12] P.E. Bak & J. von Boehm, Phys. Rev. B **21**, 5297 (1980).
- [13] R.A. Cowley & S. Bates, J. Phys. C: Solid State Phys. **21**, 4113 (1988).
- [14] O.W. Dietrich & J. Als-Nielsen, Phys. Rev. B **162**, 315 (1967).
- [15] H. Miwa & K. Yosida, Prog. Theor. Phys. **26**, 693 (1961).
- [16] S.C. Keeton & T. L. Loucks, Phys. Rev. **168**, 672 (1968).
- [17] H. Miwa, Proc. Phys. Soc. **85**, 1197 (1965).
- [18] F. Honda, N. Metoki, T.D. Matsuda, Y. Haga & Y. Onuki, J Phys. Condens. matt. **18**, 479 (2006).
- [19] R. Tróc, M. Samsel-Czekala, J. Stepień-Damm & B. Coqblin, Phys. Rev. B **85**, 224434 (2012).
- [20] L. Fast, O. Eriksson, B. Johansson et al. Phys. Rev. Lett. **81**, 2978 (1998).
- [21] T. Ueda, H. Harima, T. Yasuda, T. Kawai, R. Settai & Y. Onuki, Journal of Magnetism and Magnetic Materials **310**, 391 (2007).
- [22] M.D. Wilding & E.W. Lee, Proc. Phys. Soc. **85**, 955 (1965).
- [23] D.E. Hegland, S. Legvold & F.H. Spedding, Phys. Rev. **131**, 158 (1963).
- [24] R. Herz & H. Kronmüller, J. Magn. Mag. Mat. **9**, 273 (1978).
- [25] V.I. Zverev, A. M. Tishin, A.S. Chernyshov, Ya Mudryk, K.A. Gschneiderer & V.K. Pecharsky, J. Phys. Condes. Matter **26**, 066001 (2014).
- [26] Y. Kitano & T. Nagamiya, Prog. Theor. Phys. **31**, 1 (1964).
- [27] S. Kato, H. Kitazawa & G. Kido, Physica B **281&282** 128 (2000).
- [28] L. Benito, R.C.C. Ward & M.G. Blamire, Phys Rev B **88** 224407 (2013).
- [29] Y. Kinoshita, M. Nishino & H. Ishii, J. Phys. Soc. Japan. **71**, 3030 (2002).
- [30] C. J. Pedder, F. Krüger, A. G. Green, Phys. Rev. B **88** 165109 (2013).
- [31] Y. Sang, D. Belitz, T. R. Kirkpatrick, arXiv:1406.5745.